THE JOURNAL OF PHYSICAL CHEMISTRY C
A JOURNAL OF THE AMERICAN CHEMICAL SOCIETY

pubs.acs.org/JPCC

Article

Submonolayer Is Enough: Switching Reaction Channels on Pt/SiO_2 by Atomic Layer Deposition

Published as part of The Journal of Physical Chemistry virtual special issue "125 Years of The Journal of Physical Chemistry".

Xin Tang, Chao Liu, Edmund A. Long, Wei Lin, Ryan A. Hackler, Xiang Wang, Laurence D. Marks, Justin M. Notestein, and Peter C. Stair*

Cite This: https://doi.org/10.1021/acs.jpcc.1c04972

Read Online

ACCESS | Metrics & More | Article Recommendations | Supporting Information

ABSTRACT: The reaction mechanism of CO_2 with H_2 is studied on platinum nanoparticles supported on fumed silica. It is found that platinum nanoparticle size, reaction temperature, and metal oxide promoters play important roles in determining the reaction rate and the mechanism of forming surface carbonyl species. Metal oxide promoters consist of submonolayer titanium oxide or aluminum oxide overcoated onto the catalysts by atomic layer deposition (ALD). These alter the CO formation rate, influence the adsorption and desorption behavior, and switch the surface reaction channel from the Eley−Rideal to Langmuir−Hinshelwood mechanism due to an enhancement of CO_2 affinity to the metal−metal oxide interface. At the temperatures relevant for catalytic turnover, ALD overcoating significantly increases catalytic activity in CO_2 hydrogenation to CH_4 and CO, while the identity of the oxide overcoat helps control product selectivity.

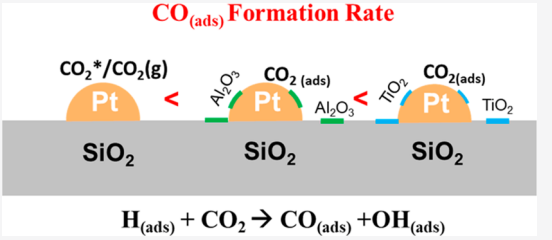

INTRODUCTION

The gas phase reaction $CO_2 + H \rightarrow CO + OH$ has been extensively studied via semiclassical and quantum dynamical simulations on multidimensional potential energy surfaces.[1−15] Key findings of the theoretical studies are that there is an "early" barrier leading to a HOCO intermediate and a "late" barrier for scission of the O−C bond.[12] By analogy to the theoretical framework from the gas phase reaction, hydrogen-assisted dissociation of carbon dioxide[16−18] may be responsible for carbonyl formation on Pt surfaces during $CO_2 + H_2$ reactions, given almost barrierless dissociation of hydrogen molecules on Pt (111) at room temperature.[19]

Overall, this process can proceed via a Langmuir−Hinshelwood (L−H) mechanism or Eley−Rideal (E−R) mechanism (Scheme 1).[20,21] In a L−H mechanism, the reaction proceeds as Pt−H + CO_2(ads) → Pt−CO + OH(ads). Because of the positive adsorption energy of CO_2 on Pt (111),[22−24] this mechanism is likely to occur only at the metal/metal oxide interface, as suggested by experimental and theoretical studies.[25] For the E−R mechanism,[26] a direct gas−solid reaction pathway is proposed: (1) Pt−H + CO_2(g)→ Pt...CO* + OH(ads), (2) Pt...CO* → Pt−CO (* represents a hot intermediate). The Eley−Rideal mechanism has been proposed for CO_2 hydrogenation on Cu (111) surfaces and Cu supported on SiO_2, where formate is observed as a product.[26,27] Because of its weak adsorption on copper and SiO_2 surfaces, gaseous CO_2 is proposed to react directly with

Scheme 1. Mechanism of $CO_2 + {}^1/_2H_2 \rightarrow CO + OH$ on Pt

Step 1:

$H_2 + 2Pt \rightarrow 2Pt\text{-}H$

Step 2:

Langmuir-Hinshelwood Mechanism

Pt-H + CO_2(ads)→ Pt-CO + OH(ads)

Eley-Rideal Mechanism

Pt-H + CO_2(g)→ Pt-CO + OH(ads)

Precursor-mediated Mechanism

Pt-H + CO_2*(ads) → Pt-CO+ OH(ads)

*(Note: * represents the excited state).*

Received: June 6, 2021
Revised: August 8, 2021

surface hydrogen atoms. Arguably, a precursor-mediated reaction could also occur,[28] where a mobile, physisorbed CO_2 molecule reacts with Pt−H to form HOCO and onward to CO(ads). This third mechanism could be viewed as an L−H mechanism where the surface CO_2 acts like a 2-D gas at the surface temperature.

For these three different reaction mechanisms, different reaction cross sections are expected, especially when a "late" barrier is present. Moreover, the fate of the reaction products from these mechanisms would be expected to differ due to their unique translational/vibrational energy distributions.[29] Therefore, it is expected to be difficult to switch between different reaction channels due to complexities in the reaction dynamics on the multidimensional potential energy surfaces.[17,30]

Atomic layer deposition (ALD) has an excellent ability to prepare nanostructures with nanometer/subnanometer precision, which carries advantages for preparing and modifying catalysts at an atomic level.[31−34] With precise control over coverages, nanoparticle sizes, and the ability to introduce specific adsorption sites, it is of interest to determine whether ALD layers may modulate reaction channels in a desirable way.[35−37] In this study, we demonstrate that a submonolayer overcoating of TiO_2 or Al_2O_3 on Pt/SiO_2, achieved by ALD, is adequate to change the reaction mechanism for surface carbonyl formation in the $CO_2 + H_2$ reaction, which ultimately influences the catalytic activity and selectivity at elevated temperatures.

EXPERIMENTAL METHODS

Fumed SiO_2 nanoparticles (AEROSIL OX 50, 50 m^2/g), were used for the support, as received. Nonporous fumed silica was specifically chosen to minimize transport limitations and to minimize the adsorption of CO_2 and formation of carbonates on the support. Pt nanoparticles (NPs) were prepared on fumed SiO_2 via ALD using $MeCpPtMe_3$ and ozone following our previously published procedure.[38] Pt loading and the Pt NP sizes were tuned by changing the number of ALD cycles, and Pt NPs samples prepared with 1, 3, and 10 cycles of ALD are named 1c-Pt/SiO_2, 3c-Pt/SiO_2, and 10c-Pt/SiO_2, respectively. The three materials had average NP sizes of 1.3, 1.6, and 4.3 nm, respectively, (see Figures S1 and S2) as determined (see below) by high-angle annular dark-field scanning transmission electron microscopy (HAADF-STEM). Total Pt surface areas were estimated as 0.004, 0.025, and 0.103 m^2/g, respectively. TiO_2 and Al_2O_3 were deposited onto Pt/SiO_2 by ALD by using one cycle of titanium isopropoxide (TTIP) and trimethylaluminum (TMA) as the metal precursors, respectively. The O precursor was deionized H_2O in both cases, and a deposition temperature of 150 °C was used. By inductively coupled plasma (ICP) elemental analysis, these conditions deposited 4.0 Al atoms/nm^2 and 2.5 Ti atoms/nm^2, consistent with prior reports.[39−41] For overcoating on 10c-Pt/SiO_2, this gives total atomic ratios of Al:Pt = 1.85:1 and Ti:Pt = 1.17:1. Because the SiO_2 surface area is much greater than the Pt surface area (50 m^2/g vs >0.1 m^2/g), the vast majority of the Al_2O_3 or TiO_2 is deposited on the SiO_2 support.

Diffuse reflectance infrared Fourier transform spectroscopy (DRIFTS) measurements were performed by using a Thermo Nicolet 6700 FTIR in the REACT core facility at Northwestern University. For a typical experiment, glass wool was loaded into a Praying Mantis IR cell, and 15−20 mg of Pt/SiO_2 was packed on top of the wool. For a typical run, the catalysts were initially raised to ∼250 °C in flowing (30 sccm) 5% O_2/Ar (UHP) to remove any residual surface carbonyls. IR spectra were measured continuously until the spectrum stabilized, indicating the removal of adsorbed CO. Spectra were recorded continuously every 9 s. Procedures for a typical experimental sequence were as follows: (1) the cell was equilibrated to the desired temperature in flowing Ar (UHP, 100 sccm), and a background spectrum was obtained; (2) 5 sccm CO_2 was added to the Ar; (3) 30 sccm of 5% H_2/Ar was added to the CO_2/Ar; (4) the gas was switched to 1% CO/N_2 (30 sccm); and (5) the gas flow was switched back to 100 sccm Ar. The catalytic activity for CO_2 hydrogenation was determined in a separate experiment using a static, batch reactor employing transmission IR spectroscopy to detect the gas phase reaction products, as described elsewhere.[42]

TEM samples were prepared by drop-casting a Pt−SiO_2/isopropyl alcohol dispersion onto holey carbon TEM grids. Grids were air-dried and then exposed to UV radiation in a vacuum for 10 min at 40% power in a ZONESEM Cleaner (Hitachi, Japan) to reduce carbon contamination arising from the dispersion.

HAADF-STEM was performed on a JEOL ARM300F Grand ARM at an accelerating voltage of 300 kV (Figure S1). Collection angles in the range 90−220 mrad were used. HAADF is an incoherent imaging technique, measuring the intensity (I) of electrons scattered to an annular detector at each pixel. The brightness of an image is proportional to the mass and the thickness of the specimen. The high collection angle means phase and diffraction contrast are generally excluded, making image interpretation relatively straightforward. Particle sizes were measured by using 50 particles from across several images in Digital Micrograph (Gatan, USA) by determining the onset of contrast changes around a particle in a HAADF image (Figure S2). Pt is much heavier than Si and O and appears much brighter in a HAADF image.

RESULTS AND DISCUSSION

$CO_2 + H_2$ on 1c-, 3c-, and 10c-Pt/SiO_2 at 25 °C. The temporal evolution of the surface carbonyl species (Pt−CO) from the reaction of $CO_2 + H_2$ was monitored, *in situ*, via DRIFTS at 25 °C for the three different sizes of Pt NPs. As described in the Experimental Methods section, the reactant gas was introduced in the following order: (1) CO_2/Ar → (2) H_2/CO_2/Ar → (3) CO/N_2 → (4) Ar, as indicated at the top of the panels in Figures 1a−c. Identical dosing procedures and durations were used in each time-dependent DRIFTS study. Figures 1a−c provide a visual depiction of the IR spectra vs time with the absorbance color-coded as shown in the scale at the right of each panel. Note that the absorbance range increases in the sequence 1(a) < 1(b) < 1(c), corresponding to the amount of CO detected. Upon CO_2 dosing at room temperature, there are no detected bands in the 1500−1900 cm^{-1} region of the DRIFTS spectra that would correspond to surface carbonate, bicarbonate, or formate species,[43,44] confirming the weak interaction of CO_2 with both Pt nanoparticles and fumed SiO_2 support. Adding H_2 to CO_2/Ar did not produce any notable surface carbonyls or other surface species, regardless of the size of Pt NPs. Switching to CO(g) revealed the presence of previously unoccupied CO adsorption sites on Pt via the infrared absorption features between 2075 and 2090 cm^{-1}, assigned to linear-bound CO.

$CO_2 + H_2$ on 1c-, 3c-, and 10c-Pt/SiO_2 at Increasing Temperature. Increasing the surface temperature is found to

https://doi.org/10.1021/acs.jpcc.1c04972
J. Phys. Chem. C XXXX, XXX, XXX−XXX

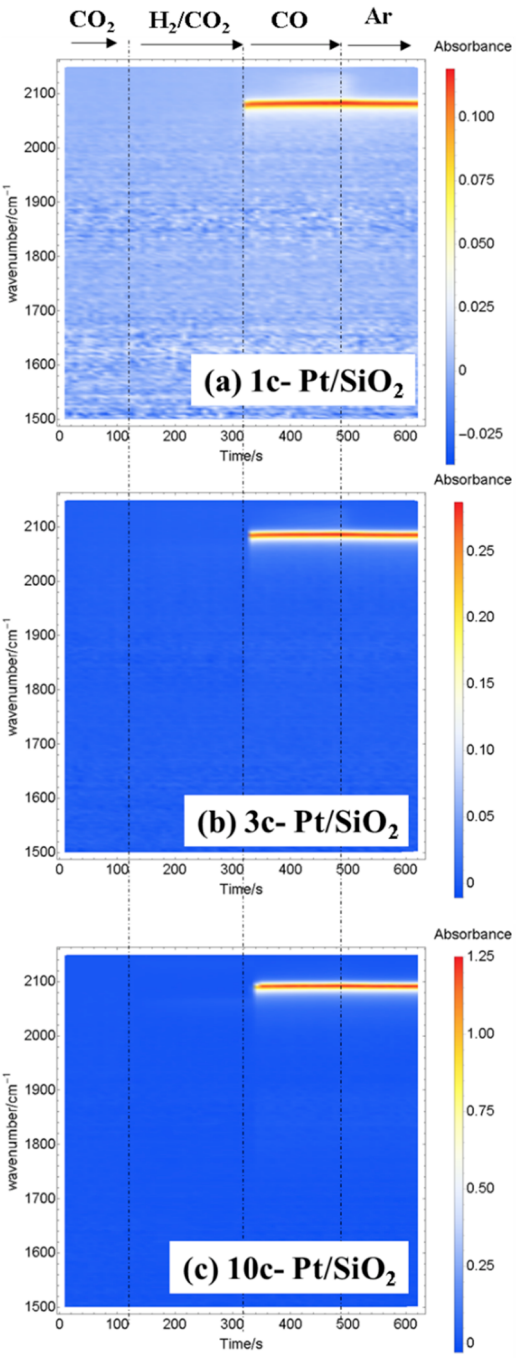

Figure 1. Time-dependent DRIFTS spectra for Pt/SiO_2 samples with different NP sizes. (a) 1c-, (b) 3c-, and (c) 10c-Pt/SiO_2 samples at 25 °C and conditions noted in the figure. Note the increase in intensity during CO adsorption from (a) to (b) to (c).

promote the formation of surface carbonyls on 1c-Pt/SiO_2, 3c-Pt/SiO_2, and 10c-Pt/SiO_2 in $CO_2 + H_2$. The formation of surface carbonyls could originate from bulk/subsurface carbonates and bicarbonates activated by higher temperature or from gas phase CO_2. Therefore, isotope-labeling experiments using $^{13}CO_2$ were also employed to confirm that Pt−^{13}CO surface carbonyls are indeed from gas phase CO_2 (see Figure S3 in the Supporting Information).

The influence of temperature on the reaction CO_2(g) to CO(ads) can be seen in the temporal evolution of surface carbonyl coverage plotted at different temperatures in Figure 2. In this figure, 1.0 monolayer is defined as the CO coverage after saturation in CO/N_2, and the same saturation level is reached independent of the temperature. For 1c-Pt/SiO_2, the formation rate of surface carbonyl is very low below 150 °C. At 150 °C and above, surface carbonyl coverage increases very rapidly until a full monolayer is achieved. For 3c-Pt/SiO_2, we observed a low formation rate for surface carbonyls below 175 °C. At 175 and 200 °C, the growth of carbonyl coverage is nearly linear versus time, indicating a constant reaction rate, independent of CO coverage up to saturation. For 10c-Pt/SiO_2, the formation of CO is slow below 200 °C. At 200, 225, and 250 °C, we again observe an approximately linear increase of CO coverage as a function of time. The linear response is maintained to almost full monolayer coverage at 225 and 250 °C.

In a typical L−H mechanism with surface carbonyls as the product, the carbonyl formation rate decreases[45] as the carbonyl coverage increases[46] due to inhibition (site occupation) by CO.[47,48] Specifically, either or both of the CO_2 or H_2 dissociative adsorption sites can be blocked by surface carbonyls in the L−H mechanism, which will lower the surface concentration of reactants and the reaction rate as the reaction proceeds. The fact that the data in Figure 2 do not exhibit product inhibition over a broad range of surface coverages is inconsistent with the L−H mechanism.

Because CO_2 does not bind strongly to either Pt nanoparticles or the SiO_2 support, the gaseous CO_2 (E−R mechanism[26]) or weakly adsorbed CO_2 (precursor-mediated mechanism) may account for the formation of surface carbonyls at elevated temperatures via reaction with Pt−H. In a previous study, King indicated that the decline in sticking coefficient is less dramatic as surface coverage increases in precursor-mediated adsorption compared to L−H chemisorption.[28] This results in a more stable reaction rate with increasing surface coverage, which is in line with our observations. However, we cannot rule out the possibility of an E−R mechanism, where no surface CO_2 species are involved, H_2 adsorption is not inhibited, and the impact of CO site occupation on CO_2 reaction is minimal regardless of coverage.

The data in Figure 2 are replotted in Figure 3a to show the surface carbonyl coverage for three samples of differently sized Pt NPs as a function of temperature during the $CO_2 + H_2$ reaction. The CO coverage is plotted after 150 s exposure to CO_2/H_2, just prior to switching to CO/N_2 at the indicated temperature. Until ∼200 °C when all the platinum NPs begin to saturate, the smaller NPs produce a higher carbonyl surface coverage in $CO_2 + H_2$ at all temperatures, indicating a higher formation rate for surface carbonyls with decreasing particle size.

The higher carbonyl formation rate on smaller nanoparticles is likely due to higher CO and CO_2 binding energies on smaller sized Pt NPs, suggesting that the CO and CO_2 binding energies may serve as descriptors for rates of carbonyl formation.[47] Indeed, a higher CO binding energy on smaller nanoparticles is supported by the work of Goodman et al., who compared the CO binding strength between different sites on Pt nanoparticles via temperature-programmed desorption (TPD) and concluded that CO binds stronger to step sites than terrace sites on platinum NPs.[49] FT-IR spectra of CO adsorbed on 1c-, 3c-, and 10c-Pt/SiO_2 (Figure 3b) showed that the peak maximum of the linear-bound CO peak (CO_L)

https://doi.org/10.1021/acs.jpcc.1c04972
J. Phys. Chem. C XXXX, XXX, XXX−XXX

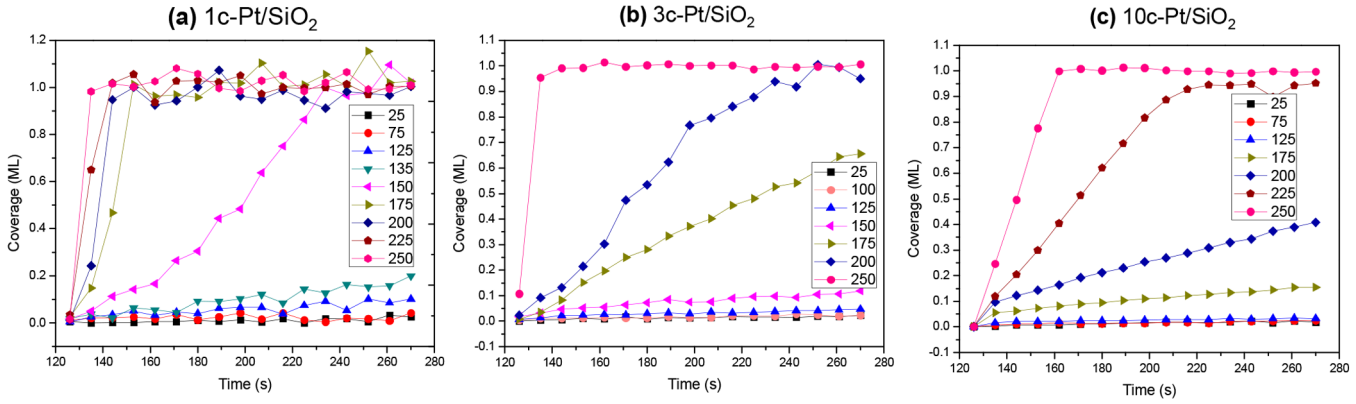

Figure 2. Time- and temperature-dependent increases in carbonyl coverage for Pt/SiO_2 materials with different NP sizes: (a) 1c-, (b) 3c-, and (c) 10c-Pt/SiO_2 in $CO_2 + H_2$. 1.0 monolayer is defined as the CO coverage after saturation in CO/N_2.

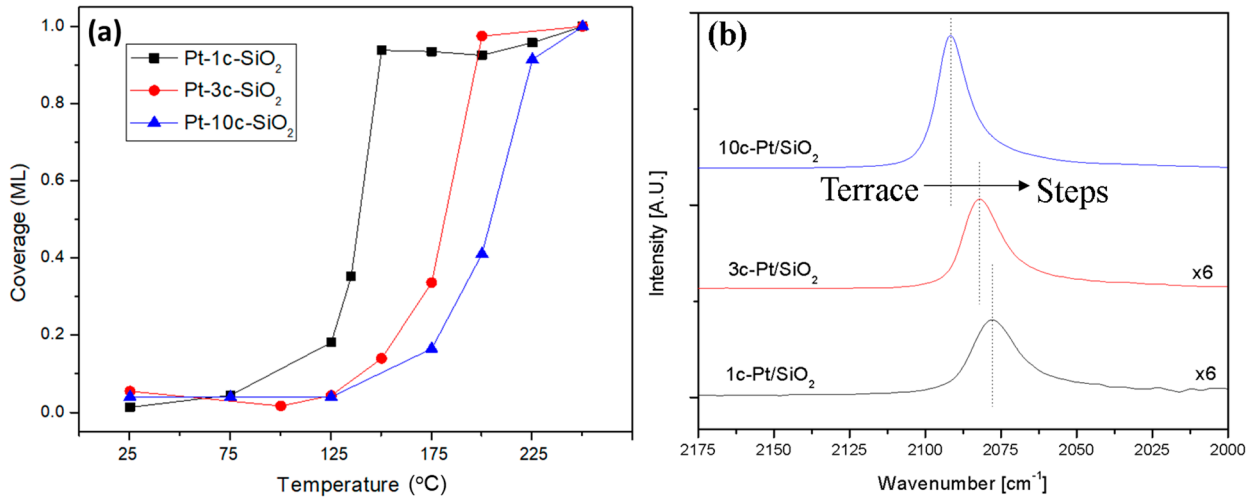

Figure 3. (a) Surface carbonyl coverage formed after 150 s exposure to CO_2/H_2 as a function of temperature. (b) IR spectra in the linear CO_L absorption region for 1c-, 3c-, and 10c-Pt/SiO_2.

shifts to higher wavenumbers as the Pt NP size increases. This blue-shift of the CO_L IR band is usually attributed to increasing dipole−dipole interactions on an extended facet, i.e., Pt (111) terrace sites[50] as well as a shift from binding on undercoordinated to well-coordinated Pt atoms.[49] For the NPs on the 1c- and 3c-Pt/SiO_2 materials, simple models of NP shape predict a higher percentage of step (undercoordinated) sites, consistent with the CO_L band at lower frequency on these smaller Pt nanoparticles.

Changes in the binding energy of CO_2 may also contribute to the NP size-dependent carbonyl formation rate.[51,52] For example, DFT calculations have shown that CO_2 binds stronger to more undercoordinated edge and corner sites than facets on Pt NPs[53] and likewise to more open Pt (100) sites than close-packed Pt (111) sites.[22] Smaller platinum nanoparticles likely contain a higher fraction of undercoordinated edge and corner sites, with more favorable CO_2 binding that accelerates the carbonyl formation reaction, if the reaction proceeds via an adsorbed, mobile precursor state.[24]

$CO_2 + H_2$ on TiO_2- and Al_2O_3-Overcoated Pt/SiO_2. Introducing one cycle of TTIP (producing TiO_2) or one cycle of TMA (producing Al_2O_3) to the 10c-Pt/SiO_2 sample results in a material where a significant carbonyl coverage is produced on the Pt NPs under a $CO_2 + H_2$ atmosphere even at room temperature (Figure 4). $^{13}CO_2$ experiments confirm that the Pt−^{13}CO surface carbonyls are from gas phase CO_2 (see Figure S3). In Figure 4, the broad absorption band at 2020−2080 cm^{-1} after the introduction of $CO_2 + H_2$ is assigned to linear-bound CO(ads), and additional weak peaks below 1900 cm^{-1} are ascribed to bridge bound CO, water bending modes, and possibly carbonates/bicarbonates (see Figure S4). Note, however, that IR absorption in the carbonate/bicarbonate region was not detectable with CO_2 alone, i.e., in the absence of H_2, and only CO_2(g) is evident in the DRIFTS spectra (see Figure S5). The saturation coverages under CO/N_2 with and without the overcoats were comparable, despite differences in bandwidth/shape and linear/bridge ratios (see Figure S6). However, ALD overcoating produced a higher CO coverage during $CO_2 + H_2$ exposure at all temperatures below 225 °C, as compared to uncoated Pt/SiO_2 (Figure 4d).

The full temporal evolution of carbonyl coverage on TiO_2- and Al_2O_3-coated catalysts is shown in Figure 5 as a function of temperature. In striking contrast to the results observed on uncoated 10c-Pt/SiO_2, the formation rate decreases as the carbonyl coverage increases. Combined with the higher surface coverages of carbonyls observed for TiO_2- or Al_2O_3-overcoated samples at any given temperature, this signifies a change in the reaction mechanism. Specifically, the apparent product

https://doi.org/10.1021/acs.jpcc.1c04972
J. Phys. Chem. C XXXX, XXX, XXX−XXX

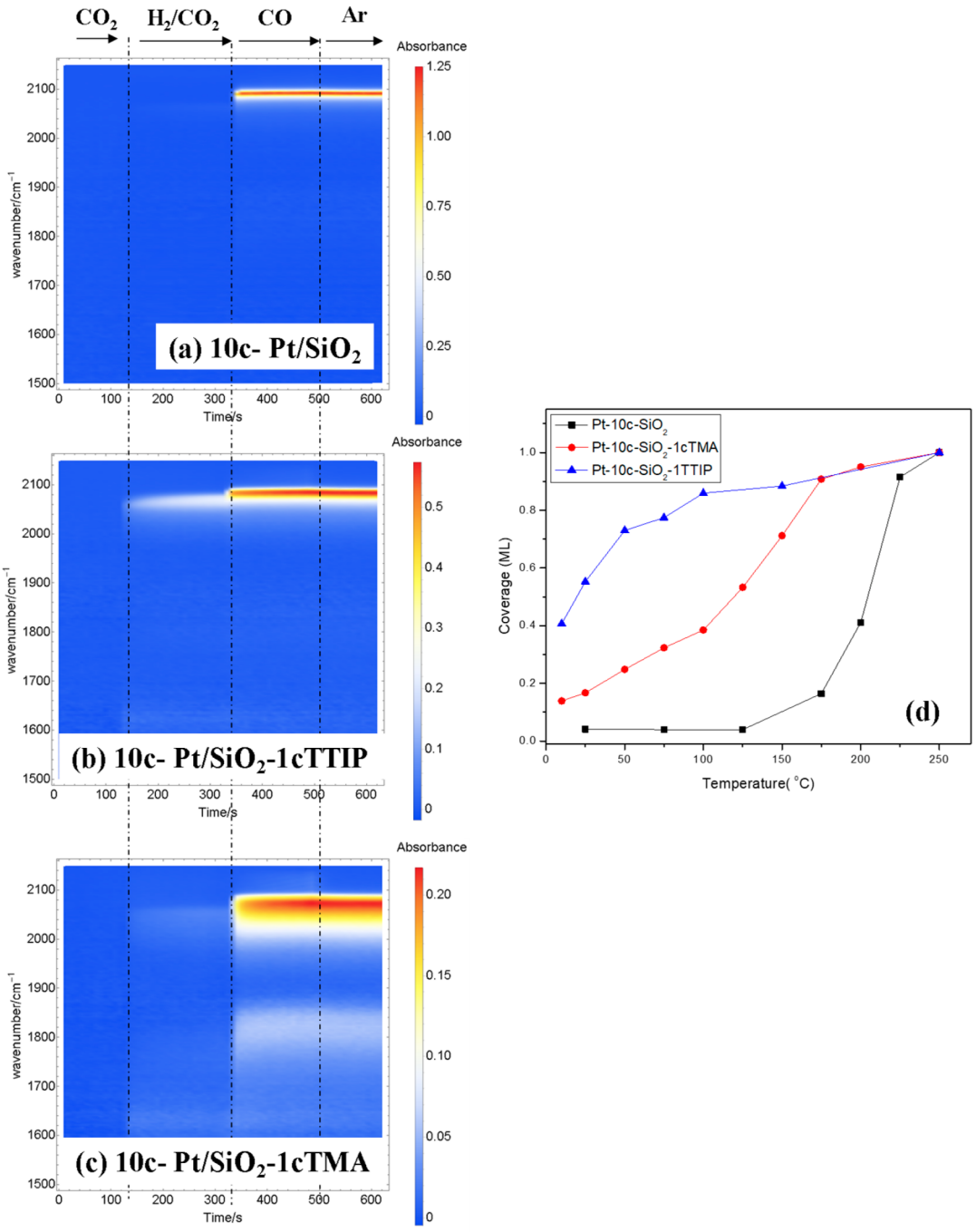

Figure 4. Time-dependent DRIFTS spectra for (a) uncoated, 10c-Pt/SiO_2, (b) TiO_2-coated, 10c-Pt/SiO_2-1cTTIP, and (c) Al_2O_3-coated, 10c-Pt/SiO_2-1cTMA at 25 °C and conditions noted in the figure. (d) Surface carbonyl coverage formed after 150 s exposure to CO_2/H_2 as a function of temperature.

inhibition is consistent with a L-H type adsorption, where the sticking coefficient decreases as more sites are occupied.[54]

While overcoating Pt/SiO_2 with TiO_2 or Al_2O_3 may, conceivably, modify the electronic structure of Pt NP in a manner analogous to a support, there is strong evidence that CO_2 adsorbed at or near the interface between Pt and the support reacts with dissociated hydrogen on platinum NPs via an L−H or a hot atom mechanism.[24,25,55] Additionally, hydrogen adsorbed at the interface may lower the barrier for CO_2 activation via an associative L−H mechanism.[56] Therefore, we attribute the enhanced CO formation rate on overcoated samples to enhanced CO_2 activation in the presence of H(ads) at the Pt−oxide interface. As the coverage of CO increases, the coverage of H(ads) decreases, leading to the product inhibition behavior characteristic of the L−H mechanism.

CO Adsorption and Desorption on TiO_2- and Al_2O_3-Coated Pt/SiO_2. In addition to their influence on accelerating CO_2 hydrogenation, both TiO_2 and Al_2O_3 overlayers also affect CO adsorption and desorption behavior on Pt NPs. TiO_2 and Al_2O_3 overcoating causes a red-shift and broadening of the CO_L band, likely due to perturbation of CO adsorption on Pt (111) facets (see Figure S6).[57] This signifies a disruption of the dipole−dipole interactions in CO adsorbed on Pt(111)

https://doi.org/10.1021/acs.jpcc.1c04972
J. Phys. Chem. C XXXX, XXX, XXX−XXX

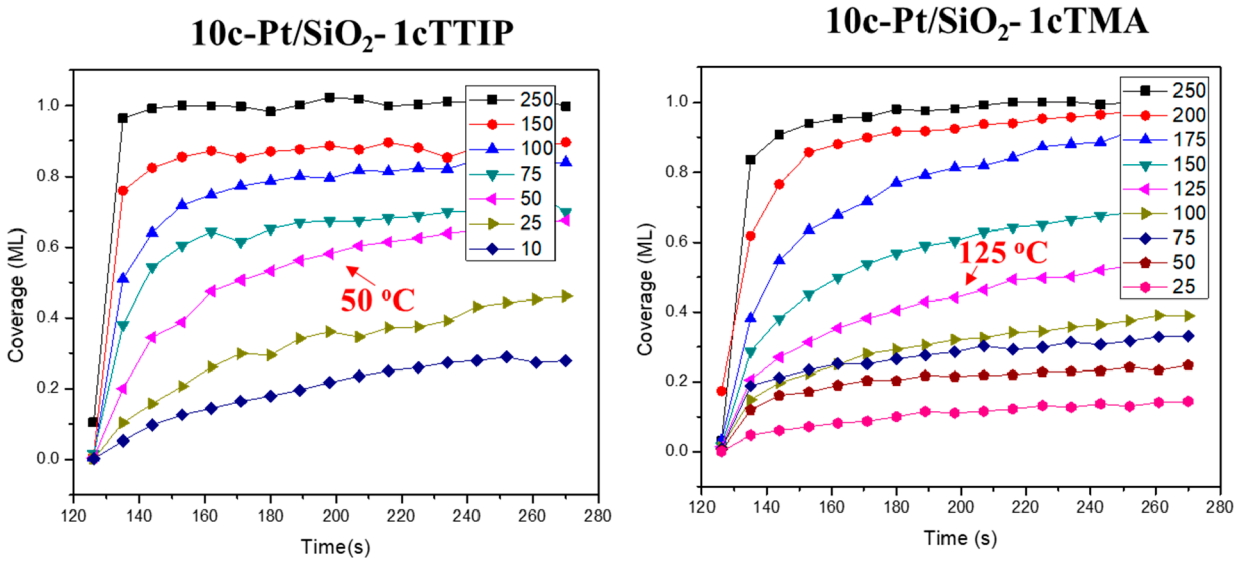

Figure 5. Temporal evolution of carbonyl coverage for TiO_2-coated (10c-Pt/SiO_2-1cTTIP) and Al_2O_3-coated (10c-Pt/SiO_2-1cTMA) materials in CO_2 + H_2 at the indicated temperatures.

facets due to the presence of oxide overlayer on the facets. Moreover, with Al_2O_3-overcoated samples, the presence of CO adsorbed at bridge sites (CO_B) was observed after introducing gas phase CO (see Figure S6). Increasing the temperature leads to comparatively smaller CO_B signal intensity (see Figure S7), which is consistent with DFT calculations showing that CO_B is less stable than CO_L on Pt (111) by about 0.12 eV.[58] Thus, the presence of an Al_2O_3 overcoat stabilizes the CO adsorption at bridge sites consistent with the presence of oxide on the Pt(111) facets.

We have also observed very different CO desorption behavior for uncoated 10c-Pt/SiO_2 compared to TiO_2- or Al_2O_3-coated Pt nanoparticles. The coverage of surface carbonyls under Ar purge for these three different cases is shown in Figure 6 as a function of time at a constant temperature of 250 °C. The CO coverage on 10c-Pt/SiO_2 can be fit to a vacancy-mediated desorption model (see equations in the Supporting Information). Initially, desorption of CO is very slow due to a lack of vacancies; once these are formed, the desorption rate (the slope of the black curve) accelerates and is proportial to $\theta_{CO(ads)} \times (1 - \theta_{CO(ads)})$.[59,60] For both Al_2O_3- and TiO_2-overcoated Pt, a much faster initial desorption rate is observed. This is consistent with less coupling of the CO dipole interactions mentioned above due to the overcoats formed by ALD. The second stage of the desorption on coated Pt is similar to that of 10c-Pt/SiO_2. This two-state behavior suggests that there are carbonyls in two different environments on the overcoated Pt/SiO_2 catalysts: CO molecules in close proximity to the overcoated oxides desorb initially with a first-order desorption kinetics while CO further away desorbs later following vacancy-mediated desorption kinetics. Indeed, the models can successfully simulate the desorption curve for CO(s) on 10c-Pt/SiO_2 and also TTIP- and TMA-coated Pt NPs. (Figure 6) Formulas for the kinetic models are provided in the Supporting Information. Interestingly, the initial desorption rate of CO on TiO_2-overcoated 10c-Pt/SiO_2 is about 2 times faster than that on Al_2O_3-overcoated Pt nanoparticles (see Table S1).

Catalytic CO_2 Hydrogenation on Uncoated Pt/SiO_2 and TiO_2- and Al_2O_3-Coated Pt/SiO_2. Surface carbonyls are

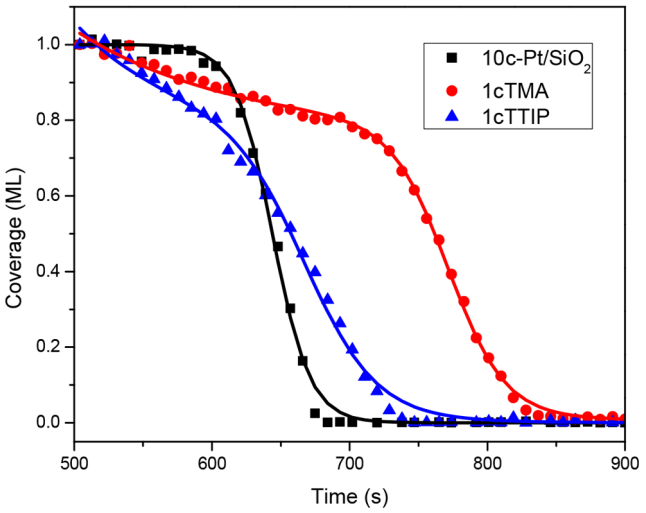

Figure 6. CO desorption during Ar purge on uncoated-, Al_2O_3-coated, and TiO_2-coated materials (10c-Pt/SiO_2, 10c-Pt/SiO_2-1cTMA, and 10c-Pt/SiO_2-1cTTIP) at 250 °C. Points are experimental data, and lines are fits to a combination of first-order desorption and vacancy-mediated desorption models. Derivations are found in the Supporting Information.

the source of gas phase CO(g) at elevated temperatures but are also available for further hydrogenation to surface carbon and hence onward to methane.[61,62] Therefore, the substantial changes in CO formation, CO adsorption, and CO desorption kinetics between the coated and uncoated Pt samples are expected to impact the overall activity and selectivity in CO_2 hydrogenation under conditions of catalytic turnover. The performance of the three catalysts for CO_2 hydrogenation was probed in a static batch reactor incorporating transmission FT-IR to detect the gas phase reaction products. Ten milligrams of catalyst was used, and 100 Torr of CO_2 and 200 Torr of H_2 were introduced into the system and reacted for 3 h at 300 °C.

The TiO_2- and Al_2O_3-coated catalysts are both more active than uncoated 10c-Pt/SiO_2 for CH_4(g) and CO(g) production, as clear from the infrared absorption bands shown in

https://doi.org/10.1021/acs.jpcc.1c04972
J. Phys. Chem. C XXXX, XXX, XXX−XXX

Figure 7. This higher catalytic activity is consistent with both their higher rates of carbonyl formation and initial CO

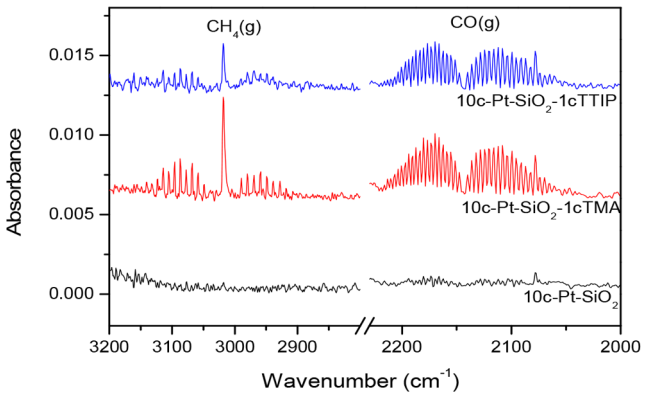

Figure 7. Transmission IR spectra of gas phase products from the reaction of CO_2 + H_2.

desorption observed in the DRIFTS experiments. Among the overcoated catalysts, the Al_2O_3-overcoated material exhibits higher selectivity toward methane than does TiO_2. As stated earlier, Al_2O_3 overcoating stabilizes more weakly bound, bridge-bonded CO and slows the initial desorption rate at 250 °C compared to TiO_2. Both factors will increase the probability of further reaction with surface hydrogen to form methane. Overall, the results demonstrate that modifying Pt/SiO_2 catalysts with submonolayer oxide overcoats can change the reaction mechanism and hence the activity and selectivity for catalytic CO_2 hydrogenation. As compared to the effect of Pt particle size, the influence of surface modification is much more pronounced.

CONCLUSIONS

In summary, submonolayer ALD overcoating of Pt nanoparticles supported on SiO_2 can modulate the temperature/time-dependent formation of surface carbonyls by activating CO_2 dissociation. For uncoated Pt/SiO_2, an E−R mechanism or mobile precursor mediated mechanism is likely responsible for surface carbonyl formation, and the size of platinum nanoparticles dictates rates by controlling the CO/CO_2 binding energies. Overcoat modification of Pt/SiO_2 boosts the catalytic activity by increasing the CO formation and desorption rates and providing more interfacial sites. TiO_2 and Al_2O_3 overcoats produce both CH_4 and CO; Al_2O_3 overcoats stabilize weak CO adsorption sites and give slower initial CO desorption rates, correlating with its higher methane selectivity. Atomic layer deposition is a promising tool to investigate reaction mechanisms and to modulate reaction pathways by changing the variables that determine reactive processes, i.e., binding energy, adsorption strengths, and interfaces.

ASSOCIATED CONTENT

Supporting Information

The Supporting Information is available free of charge at https://pubs.acs.org/doi/10.1021/acs.jpcc.1c04972.

HAADF characterizations of supported Pt nanoparticle, isotope-labeling experiments, additional DRIFTS spectra of uncoated and coated Pt/SiO_2 in CO_2 + H_2, CO_2 and CO and fitted equations and rate constant for CO desorption kinetics (PDF)

AUTHOR INFORMATION

Corresponding Author

Peter C. Stair − *Department of Chemistry, Northwestern University, Evanston, Illinois 60208, United States;* orcid.org/0000-0001-5654-6000; Email: pstair@northwestern.edu

Authors

Xin Tang − *Department of Chemistry, Northwestern University, Evanston, Illinois 60208, United States*

Chao Liu − *Department of Chemical and Biological Engineering, Northwestern University, Evanston, Illinois 60208, United States*

Edmund A. Long − *Department of Materials Science and Engineering, Northwestern University, Evanston, Illinois 60208, United States*

Wei Lin − *Department of Chemistry, Northwestern University, Evanston, Illinois 60208, United States;* orcid.org/0000-0002-5046-4765

Ryan A. Hackler − *Department of Chemistry, Northwestern University, Evanston, Illinois 60208, United States;* orcid.org/0000-0003-4698-6074

Xiang Wang − *Department of Chemistry, Northwestern University, Evanston, Illinois 60208, United States;* orcid.org/0000-0003-1322-7071

Laurence D. Marks − *Department of Materials Science and Engineering, Northwestern University, Evanston, Illinois 60208, United States;* orcid.org/0000-0002-6659-2016

Justin M. Notestein − *Department of Chemical and Biological Engineering, Northwestern University, Evanston, Illinois 60208, United States;* orcid.org/0000-0003-1780-7356

Complete contact information is available at: https://pubs.acs.org/10.1021/acs.jpcc.1c04972

Notes

The authors declare no competing financial interest.

ACKNOWLEDGMENTS

This material is based upon work supported by the Institute for Catalysis in Energy Processes (ICEP) at Northwestern University under U.S. Department of Energy, Office of Science, Office of Basic Energy Sciences Award DOE DE-FG02-03-ER15457.

REFERENCES

(1) Brunning, J.; Derbyshire, D. W.; Smith, I. W. M.; Williams, M. D. Kinetics of OH(v = 0,1) and OD(v = 0,1) with CO and the Mechanism of the OH + CO Reaction. *J. Chem. Soc., Faraday Trans. 2* **1988**, *84*, 105−119.

(2) Scherer, N. F.; Sipes, C.; Bernstein, R. B.; Zewail, A. H. Real-Time Clocking of Bimolecular Reactions: Application to H+CO_2. *J. Chem. Phys.* **1990**, *92*, 5239−5259.

(3) Alagia, M.; Balucani, N.; Casavecchia, P.; Stranges, D.; Volpi, G. G. Crossed Beam Studies of Four-Atom Reactions: The Dynamics of OH+CO. *J. Chem. Phys.* **1993**, *98*, 8341−8344.

(4) Bowman, J. M.; Schatz, G. C. Theoretical Studies of Polyatomic Bimolecular Reaction Dynamics. *Annu. Rev. Phys. Chem.* **1995**, *46*, 169−196.

(5) Zhang, D. H.; Zhang, J. Z. H. Quantum Calculations of Reaction Probabilities for HO + CO - H + CO_2 and Bound States of HOCO. *J. Chem. Phys.* **1995**, *103*, 6512−6519.

(6) Yu, H. G.; Muckerman, J. T.; Sears, T. J. A Theoretical Study of the Potential Energy Surface for the Reaction OH + CO - H + CO_2. *Chem. Phys. Lett.* **2001**, *349*, 547−554.

https://doi.org/10.1021/acs.jpcc.1c04972
J. Phys. Chem. C XXXX, XXX, XXX−XXX

(7) Lakin, M. J.; Troya, D.; Schatz, G. C.; Harding, L. B. A Quasiclassical Trajectory Study of the Reaction OH + CO - H + CO_2. *J. Chem. Phys.* **2003**, *119*, 5848−5859.
(8) Valero, R.; Kroes, G. J. Role of CO Vibration in the Complex-Forming OH + CO - H + CO_2 Reaction. *Phys. Rev. A: At., Mol., Opt. Phys.* **2004**, *70*, 040701.
(9) Francisco, J. S.; Muckerman, J. T.; Yu, H. G. HOCO Radical Chemistry. *Acc. Chem. Res.* **2010**, *43*, 1519−1526.
(10) Liu, S.; Xu, X.; Zhang, D. H. Communication: State-to-State Quantum Dynamics Study of the OH + CO - H + CO_2 Reaction in Full Dimensions (J = 0). *J. Chem. Phys.* **2011**, *135*, 141108.
(11) Guo, H. Quantum Dynamics of Complex-Forming Bimolecular Reactions. *Int. Rev. Phys. Chem.* **2012**, *31*, 1−68.
(12) Li, J.; Wang, Y.; Jiang, B.; Ma, J.; Dawes, R.; Xie, D.; Bowman, J. M.; Guo, H. Communication: A Chemically Accurate Global Potential Energy Surface for the HO + CO - H + CO_2 Reaction. *J. Chem. Phys.* **2012**, *136*, 041103.
(13) Li, J.; Xie, C.; Ma, J.; Wang, Y.; Dawes, R.; Xie, D.; Bowman, J. M.; Guo, H. Quasi-Classical Dynamics of the HO + CO - H + CO_2 Reaction on a New Ab Initio Based Potential Energy Surface. *J. Phys. Chem. A* **2012**, *116*, 5057−5067.
(14) Ma, J.; Li, J.; Guo, H. Quantum Dynamics of the HO + CO - H + CO_2 Reaction on an Accurate Potential Energy Surface. *J. Phys. Chem. Lett.* **2012**, *3*, 2482−2486.
(15) Xie, C.; Li, J.; Xie, D.; Guo, H. Quasi-Classical Trajectory Study of the H + CO_2 - HO + CO Reaction on a New ab Initio Based Potential Energy Surface. *J. Chem. Phys.* **2012**, *137*, 024308.
(16) Lin, W.; Stocker, K. M.; Schatz, G. C. Mechanisms of Hydrogen-Assisted CO_2 Reduction on Nickel. *J. Am. Chem. Soc.* **2017**, *139*, 4663−4666.
(17) Lin, W.; Stocker, K. M.; Schatz, G. C. Reducing CO_2 to CO and H_2O on Ni(110): The Influence of Subsurface Hydrogen. *J. Phys. Chem. C* **2016**, *120*, 23061−23068.
(18) Peng, G.; Sibener, S. J.; Schatz, G. C.; Mavrikakis, M. CO_2 Hydrogenation to Formic Acid on Ni(110). *Surf. Sci.* **2012**, *606*, 1050−1055.
(19) Arboleda, N. B.; Kasai, H.; Dino, W. A.; Nakanishi, H. Potential Energy of H_2 Dissociation and Adsorption on Pt(111) Surface: First-Principles Calculation. *Jpn. J. Appl. Phys.* **2007**, *46*, 4233.
(20) Rettner, C. T.; Auerbach, D. J. Distinguishing the Direct and Indirect Products of a Gas-Surface Reaction. *Science* **1994**, *263*, 365−367.
(21) Quattrucci, J. G.; Jackson, B. Quasiclassical study of Eley-Rideal and hot atom reactions of H atoms with Cl adsorbed on a Au(111) surface. *J. Chem. Phys.* **2005**, *122*, 074705.
(22) Liu, X.; Sun, L.; Deng, W.-Q. Theoretical Investigation of CO_2 Adsorption and Dissociation on Low Index Surfaces of Transition Metals. *J. Phys. Chem. C* **2018**, *122*, 8306−8314.
(23) Phatak, A. A.; Koryabkina, N.; Rai, S.; Ratts, J. L.; Ruettinger, W.; Farrauto, R. J.; Blau, G. E.; Delgass, W. N.; Ribeiro, F. H. Kinetics of the Water-gas Shift Reaction on Pt Catalysts Supported on Alumina and Ceria. *Catal. Today* **2007**, *123*, 224−234.
(24) Kattel, S.; Liu, P.; Chen, J. G. Tuning Selectivity of CO_2 Hydrogenation Reactions at the Metal/Oxide Interface. *J. Am. Chem. Soc.* **2017**, *139*, 9739−9754.
(25) Goguet, A.; Meunier, F. C.; Tibiletti, D.; Breen, J. P.; Burch, R. Spectrokinetic Investigation of Reverse Water-Gas-Shift Reaction Intermediates over a Pt/CeO_2 Catalyst. *J. Phys. Chem. B* **2004**, *108*, 20240−20246.
(26) Nakano, H.; Nakamura, I.; Fujitani, T.; Nakamura, J. Structure-Dependent Kinetics for Synthesis and Decomposition of Formate Species over Cu(111) and Cu(110) Model Catalysts. *J. Phys. Chem. B* **2001**, *105*, 1355−1365.
(27) Wang, G.; Morikawa, Y.; Matsumoto, T.; Nakamura, J. Why Is Formate Synthesis Insensitive to Copper Surface Structures? *J. Phys. Chem. B* **2006**, *110*, 9−11.
(28) King, D. A.; Wells, M. G. Reaction Mechanism in Chemisorption Kinetics: Nitrogen on the {100} Plane of Tungsten. *Proc. R. Soc. Lond. A.* **1974**, *339*, 245−269.
(29) Rettner, C. T.; Auerbach, D. J.; Tully, J. C.; Kleyn, A. W. Chemical Dynamics at the Gas- surface Interface. *J. Phys. Chem.* **1996**, *100*, 13021−13033.
(30) Rodriguez, J. A.; Liu, P.; Stacchiola, D. J.; Senanayake, S. D.; White, M. G.; Chen, J. G. Hydrogenation of CO_2 to Methanol: Importance of Metal-Oxide and Metal−Carbide Interfaces in the Activation of CO_2. *ACS Catal.* **2015**, *5*, 6696−6706.
(31) O'Neill, B. J.; Jackson, D. H. K.; Lee, J.; Canlas, C.; Stair, P. C.; Marshall, C. L.; Elam, J. W.; Kuech, T. F.; Dumesic, J. A.; Huber, G. W. Catalyst Design with Atomic Layer Deposition. *ACS Catal.* **2015**, *5*, 1804−1825.
(32) Lu, J.; Fu, B.; Kung, M. C.; Xiao, G.; Elam, J. W.; Kung, H. H.; Stair, P. C. Coking- and Sintering-Resistant Palladium Catalysts Achieved Through Atomic Layer Deposition. *Science* **2012**, *335*, 1205−1208.
(33) Christensen, S. T.; Feng, H.; Libera, J. L.; Guo, N.; Miller, J. T.; Stair, P. C.; Elam, J. W. Supported Ru-Pt Bimetallic Nanoparticle Catalysts Prepared by Atomic Layer Deposition. *Nano Lett.* **2010**, *10*, 3047−3051.
(34) Wegener, S. L.; Marks, T. J.; Stair, P. C. Design Strategies for the Molecular Level Synthesis of Supported Catalysts. *Acc. Chem. Res.* **2012**, *45*, 206−214.
(35) Feng, H.; Elam, J. W.; Libera, J. A.; Setthapun, W.; Stair, P. C. Palladium Catalysts Synthesized by Atomic Layer Deposition for Methanol Decomposition. *Chem. Mater.* **2010**, *22*, 3133−3142.
(36) Lu, J.; Elam, J. W.; Stair, P. C. Synthesis and Stabilization of Supported Metal Catalysts by Atomic Layer Deposition. *Acc. Chem. Res.* **2013**, *46*, 1806−1815.
(37) Yan, H.; He, K.; Samek, I. A.; Jing, D.; Nanda, M. G.; Stair, P. C.; Notestein, J. M. Tandem In_2O_3-Pt/Al_2O_3 Catalyst for Coupling of Propane Dehydrogenation to Selective H_2 Combustion. *Science* **2021**, *371*, 1257−1260.
(38) Christensen, S. T.; Elam, J. W.; Rabuffetti, F. A.; Ma, Q.; Weigand, S. J.; Lee, B.; Seifert, S.; Stair, P. C.; Poeppelmeier, K. R.; Hersam, M. C.; Bedzyk, M. J. Controlled Growth of Platinum Nanoparticles on Strontium Titanate Nanocubes by Atomic Layer Deposition. *Small* **2009**, *5*, 750−757.
(39) Hackler, R. A.; Kang, G.; Schatz, G. C.; Stair, P. C.; Van Duyne, R. P. Analysis of TiO_2 Atomic Layer Deposition Surface Chemistry and Evidence of Propene Oligomerization Using Surface-Enhanced Raman Spectroscopy. *J. Am. Chem. Soc.* **2019**, *141*, 414−422.
(40) Hackler, R. A.; McAnally, M. O.; Schatz, G. C.; Stair, P. C.; Van Duyne, R. P. Identification of Dimeric Methylalumina Surface Species during Atomic Layer Deposition Using Operando Surface-Enhanced Raman Spectroscopy. *J. Am. Chem. Soc.* **2017**, *139*, 2456−2463.
(41) Kennedy, R. M.; Crosby, L. A.; Ding, K.; Canlas, C. P.; Gulec, A.; Marks, L. D.; Elam, J. W.; Marshall, C. L.; Poeppelmeier, K. R.; Stair, P. C. Replication of SMSI via ALD: TiO_2 Overcoats Increase Pt-Catalyzed Acrolein Hydrogenation Selectivity. *Catal. Lett.* **2018**, *148*, 2223−2232.
(42) Liu, C.; Notestein, J. M.; Weitz, E.; Gray, K. A. Photo-Initiated Reduction of CO_2 by H_2 on Silica Surface. *ChemSusChem* **2018**, *11*, 1163−1168.
(43) Turek, A. M.; Wachs, I. E.; DeCanio, E. Acidic Properties of Alumina-supported Metal Oxide Catalysts: an Infrared Spectroscopy Study. *J. Phys. Chem.* **1992**, *96*, 5000−7.
(44) Calatayud, M.; Collins, S. E.; Baltanas, M. A.; Bonivardi, A. L. Stability of Formate Species on β-Ga_2O_3. *Phys. Chem. Chem. Phys.* **2009**, *11*, 1397−1405.
(45) Eiswirth, M.; Bürger, J.; Strasser, P.; Ertl, G. Oscillating Langmuir-Hinshelwood Mechanisms. *J. Phys. Chem.* **1996**, *100*, 19118−19123.
(46) Daza, Y. A.; Kuhn, J. N. CO_2 Conversion by Reverse Water Gas Shift Catalysis: Comparison of Catalysts, Mechanisms and their Consequences for CO_2 Conversion to Liquid Fuels. *RSC Adv.* **2016**, *6*, 49675−49691.
(47) Plazinski, W.; Rudzinski, W.; Plazinska, A. Theoretical Models of Sorption Kinetics Including a Surface Reaction Mechanism: A Review. *Adv. Colloid Interface Sci.* **2009**, *152*, 2−13.

https://doi.org/10.1021/acs.jpcc.1c04972
J. Phys. Chem. C XXXX, XXX, XXX−XXX

(48) Liu, Y.; Shen, L. From Langmuir Kinetics to First- and Second-Order Rate Equations for Adsorption. *Langmuir* **2008**, *24*, 11625−11630.
(49) Lundwall, M. J.; McClure, S. M.; Goodman, D. W. Probing Terrace and Step Sites on Pt Nanoparticles Using CO and Ethylene. *J. Phys. Chem. C* **2010**, *114*, 7904−7912.
(50) Ding, K.; Gulec, A.; Johnson, A. M.; Schweitzer, N. M.; Stucky, G. D.; Marks, L. D.; Stair, P. C. Identification of Active Sites in CO Oxidation and Water-gas Shift over Supported Pt Catalysts. *Science* **2015**, *350*, 189−192.
(51) Liu, Q.; Yang, X.; Li, L.; Miao, S.; Li, Y.; Li, Y.; Wang, X.; Huang, Y.; Zhang, T. Direct Catalytic Hydrogenation of CO_2 to Formate over a Schiff-base-mediated Gold Nanocatalyst. *Nat. Commun.* **2017**, *8*, 1407.
(52) Kattel, S.; Yan, B.; Yang, Y.; Chen, J. G.; Liu, P. Optimizing Binding Energies of Key Intermediates for CO_2 Hydrogenation to Methanol over Oxide-Supported Copper. *J. Am. Chem. Soc.* **2016**, *138*, 12440−12450.
(53) Kattel, S.; Yan, B. H.; Chen, J. G. G.; Liu, P. CO_2 Hydrogenation on Pt, Pt/SiO_2 and Pt/TiO_2: Importance of Synergy between Pt and Oxide Support. *J. Catal.* **2016**, *343*, 115−126.
(54) Villa de P, A. d. L.; Taborda A, F.; Montes de Correa, C. Kinetics of Limonene Epoxidation by Hydrogen Peroxide on PW-Amberlite. *J. Mol. Catal. A: Chem.* **2002**, *185*, 269−277.
(55) Jin, T.; Zhou, Y.; Mains, G. J.; White, J. M. Infrared and X-ray Photoelectron Spectroscopy Study of Carbon Monoxide and Carbon Dioxide on Platinum/ceria. *J. Phys. Chem.* **1987**, *91*, 5931−5937.
(56) Kattel, S.; Ramírez, P. J.; Chen, J. G.; Rodriguez, J. A.; Liu, P. Active Sites for CO_2 Hydrogenation to Methanol on Cu/ZnO catalysts. *Science* **2017**, *355*, 1296−1299.
(57) Kale, M. J.; Christopher, P. Utilizing Quantitative in Situ FTIR Spectroscopy To Identify Well-Coordinated Pt Atoms as the Active Site for CO Oxidation on Al_2O_3-Supported Pt Catalysts. *ACS Catal.* **2016**, *6*, 5599−5609.
(58) Feibelman, P. J.; Hammer, B.; Nørskov, J. K.; Wagner, F.; Scheffler, M.; Stumpf, R.; Watwe, R.; Dumesic, J. The CO/Pt(111) Puzzle. *J. Phys. Chem. B* **2001**, *105*, 4018−4025.
(59) Mhatre, B. S.; Pushkarev, V.; Holsclaw, B.; Lawton, T. J.; Sykes, E. C. H.; Gellman, A. J. A Window on Surface Explosions: Tartaric Acid on Cu(110). *J. Phys. Chem. C* **2013**, *117*, 7577−7588.
(60) Gellman, A. J.; Huang, Y.; Feng, X.; Pushkarev, V. V.; Holsclaw, B.; Mhatre, B. S. Superenantioselective Chiral Surface Explosions. *J. Am. Chem. Soc.* **2013**, *135*, 19208−19214.
(61) Wang, X.; Shi, H.; Kwak, J. H.; Szanyi, J. Mechanism of CO_2 Hydrogenation on Pd/Al_2O_3 Catalysts: Kinetics and Transient DRIFTS-MS Studies. *ACS Catal.* **2015**, *5*, 6337−6349.
(62) Wang, X.; Shi, H.; Szanyi, J. Controlling Selectivities in CO_2 Reduction through Mechanistic Understanding. *Nat. Commun.* **2017**, *8*, 513.

https://doi.org/10.1021/acs.jpcc.1c04972
J. Phys. Chem. C XXXX, XXX, XXX−XXX